Determining effects of spacer orientations on channel hydraulic conditions using PIV

Haidari, A. H.; Heijman, S. G.J.; Uijttewaal, W. S.J.; van der Meer, W. G.J.

Important note
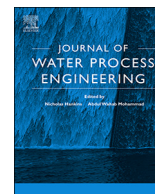To cite this publication, please use the final published version (if applicable).
Please check the document version above.

Determining effects of spacer orientations on channel hydraulic conditions using PIV

A.H. Haidari[a,*], S.G.J. Heijman[a], W.S.J. Uijttewaal[a], W.G.J. van der Meer[a,b,c]

[a] *Delft University of Technology, Department of Civil Engineering, Stevinweg 01, 2628 CN Delft, the Netherlands*
[b] *Oasen, P.O. Box 122, 2800 AC Gouda, the Netherlands*
[c] *University of Twente, Faculty of Science and Technology, Drienerlolaan 5, 7522 NB Enschede, the Netherlands*

ARTICLE INFO

ABSTRACT

Feed spacer orientation affects the velocity pattern and pressure drop of spacer-filled channels such as those encountered in Spiral-wound Membrane (SWM) modules of Reverse Osmosis (RO). However, there are only limited numbers of experimental studies on this topic. This study sets out to reveal more detailed information on the pressure drop and velocity patterns of spacer-filled channels. Particle Image Velocimetry (PIV) is used to provide high-resolution velocity maps for three commercial feed spacers of different thicknesses at a flow attack angle of 45° and 90°. The pressure drop is measured for the applied operational conditions (Re < 250). Results showed higher pressure losses, a better mixing of flow, a lower variation of temporal velocity, and a smaller variation of velocity over the channel height in the orientation with a flow attack angle of 45° as compared to 90°. The results presented here can be used to validate numerical studies, determine the fouling-sensitive regions in a spacer-filled channel and consequently, design the optimal spacer with respect to its orientation and thickness.

1. Introduction

Reverse Osmosis (RO) has become a popular technology around the world for production of highly purified water [1]. The coming decades are likely to witness an even greater use of RO for purification of fresh surface water as a consequence of the emergence of new types of micropollutants such as drug residues in fresh water, which cannot be removed with conventional treatment plants. For instance, Wong et al. [2,3] reported that certain species are in danger of extinction in almost half of European and North American rivers and lakes because of the pollution of these ecosystems [4].

The Spiral-Wound Membrane (SWM) configuration is the most common configuration applied in Nanofiltration (NF) and RO because it offers a good balance between ease of operation, fouling control, permeation rate, and packing density [5–8]. However, a wider and more efficient application of SWM configuration requires further improvements of the module's components such as the feed spacer [3,9–12]. The feed spacer works as a supporting net and keeps two adjacent envelopes apart [13,14]; it thereby provides a passing channel for feed water to move tangentially over the active layer of membrane sheets [15]. In addition, the feed spacer determines the hydraulic conditions of

the feed channel such as the pressure drop and the time and location of initiation of the fouling. Thus, any alteration in geometrical characteristics of the feed spacer results in the changing of hydraulic conditions of the SWM module.

A slight increase in the thickness of the feed spacer (from 28 to 34 mils) is one of the few changes that feed spacers have undergone since the first design of SWM modules of RO. This improvement led to the manufacturing of low-pressure RO modules. At a constant production rate, low-pressure modules have a lower fouling tendency and pressure drop [16] and consequently consume less energy compared to modules composed of 28 mils (0.7 mm) spacers. Such improvements are particularly attractive when fresh water is used as the feed for SWM modules of RO because of a higher ratio of pressure losses to applied pressure in fresh water. This higher ratio can be explained by the fact that the applied pressure in fresh water is lower than brackish water and seawater due to its lower osmotic pressure, but the pressure drop along a (clean) SWM module is the same for all types of water due to constant geometrical characteristics of the feed spacer and feed channel in commercial modules.

Considering the amount of water produced by RO plants worldwide and high energy costs, even a small improvement in the efficiency of

---

Nomenclature

A	The cross-section area of the feed channel m^2
A', n	Constants in the friction factor dependency on Reynolds number
A$_{eff}$	The cross-section area of the feed channel involving the spacer porosity m^2
C$_{td}$	Darcy-Weisbach factor, Manning friction factor, or total drag
d$_{f1}$	Thickness of filament of spacer in parallel direction of the flow m
d$_{f2}$	Thickness of filament of spacer in perpendicular direction of the flow m
d$_H$	Hydraulic diameter m
dp	Pressure drop pa
h$_{sp}$	Thickness of feed spacer m
H$_{CH}$	Height of the feed channel m
K, m	Constants in the pressure drop dependency on velocity
L	Length of the feed channel m
l$_{m1}$	Mesh length of spacer in direction parallel to flow m
l$_{m2}$	Mesh length of spacer in direction perpendicular to flow m
Q	Flow m^3/s
S$_{v,sp}$	the specific surface of the spacer
U$_{aver}$	Average velocity m/s
U$_{sup}$	Superficial velocity m/s
V$_{sp}$	Volume of spacer in a mesh m^3
V$_{mesh}$	Total volume of a mesh m^3
W	Width of the feed channel m

X	The flow direction
Y	Direction perpendicular to flow but not in direction of channel height
Z	Direction perpendicular to flow and in the direction of the channel height
Z1	plane close to the membrane surface
Z2	plane close to the middle of the feed channel at the boundary of top and bottom filaments
Z3	Plane close to Plexiglas surface or close to observation window

Greek symbols

α	Spacer's flow attack angle ^{O}
β	Spacer's angle or Hydrodynamic angle of spacer ^{O}
ε	Porosity of spacer filled-channel -
μ	Dynamic viscosity of the fluid kg/(m.s)
ρ	Density of the water kg/m^3

Abbreviations

CFD	Computational fluid dynamics
FOV	Field of view
PIV	Particle image velocimetry
Re	Reynolds number
Re$_h$	Hydraulic Reynolds number
RO	Reverse osmosis
SWM	Spiral-wound membrane

the feed spacer can be translated into large savings or increased water output [17]. Therefore, it is crucial to understand the effects of geometric modification of the feed spacer on hydraulic conditions of the feed channel, such as the pressure drop and the velocity pattern.

While many studies have investigated the effect of feed spacer geometry on the energy losses and the hydrodynamics inside the feed channel, only a few have addressed the effects of orientation. The orientation of a feed spacer is determined by the flow attack angle (α), which is defined as the angle between the flow and hydrodynamic angle (β) of the spacer (Fig. 1). The hydrodynamic angle is the interior angle, relative to feed flow, at the intersection of longitudinal and transverse filaments.
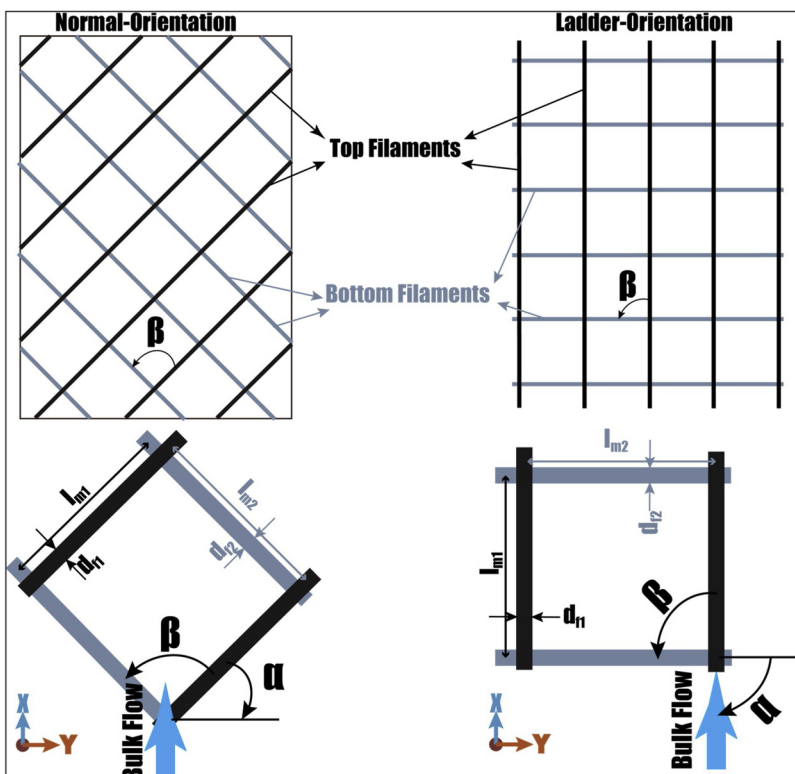
Fig. 1. Schematic view of spacers with flow attack angle of 45° (normal orientation) and 90° (ladder orientation). The flow attack angle is denoted with α and the hydrodynamic angle with β. The relative distance between axes of two consecutive spacer filaments is defined as the ratio of filament length (lm = lm1 = lm2) to the channel height (H$_{CH}$). Spacers used in this article have the same filament mesh in flow direction (lm1) and perpendicular to the flow (lm2). The XY-plane is defined as the 2D space that represents the direction of flow in X- and Y-direction. X denotes the main direction of the flow (x-component of flow), and Y denotes the flow direction perpendicular to the main flow and perpendicular to the channel height (Z).

Zimmere and Kottke [15] studied effects of the flow attack angle (α) and the ratio of filaments length to channel height (l_m/H_{CH}) on the pressure drop, mass transfer, and mixing behavior of flow by physiochemical principles using ammonia. In addition, they used a tracer of ammonia for visualization of the flow and of the mass transfer inhomogeneity in the feed channel. They concluded that a proper choice of the l_m/H_{CH} ratio and the flow attack angle (orientation) of the feed spacer results in overlapping of two basic flow types (channel flow and corkscrew flow) and creation of mixing by which a homogeneous mass transfer combined with a good residence time behavior at acceptable energy costs could be achieved. Geraldes et al. [18] investigated the effect of l_m/H_{CH} ratio in a ladder type feed spacer and found that the value of the Reynolds number at which the flow becomes unstable decreases due to the increase of inter-filament distance between two transverse filaments. Santos et al. [19] used experimental and numerical studies to determine the shear stress and the mass transfer at the membrane wall for ladder-oriented spacers. They introduced a modified friction factor and found that it is linearly related to the Sherwood number. Based on this linear relation, they suggested that the modified friction factor may be used for selecting the best spacers in terms of mass transfer efficiency. Additionally, they showed that the flow structure is mainly affected by transverse filaments and that effects of longitudinal filaments are marginal. Li et al. [20] used a CFD simulation to calculate the mass transfer and power consumption of non-woven spacers at different l_m/H_{CH} ratio, flow attack angle, and hydrodynamic angle. They concluded that there should be an optimum value for the l_m/H_{CH} ratio, the hydrodynamic angle, and the flow attack angle. Koutsou et al. [21] performed experimental and numerical simulation at a typical Reynolds number for RO (50 < Re < 200). They investigated the effect of both Reynolds (Re) and Schmidt (Sc) numbers on the Sherwood (Sh) number in spacer-filled channels by changing the l_m/H_{CH} ratio, the flow attack angle, and the hydrodynamic angle of spacers. They demonstrated that the local mass transfer was lower in sparser spacer geometries, but increased by increasing the hydrodynamic angle. Additionally, they showed that the distribution of average mass transfer was similar to the corresponding distribution of shear stress at the channel walls.

While the previously mentioned researchers used spacers with a simplified cross-section for numerical simulations, more recent numerical studies, e.g. studies done by Bucs et al. [22] and Radu et al. [23], have started to use spacers with closer geometrical similarities to those of commercial ones. However, it remains a challenge in numerical methods to use spacers with a geometry that exactly matches the geometry of commercial spacers, and therefore, the use of feed spacers with detailed geometry, such as the commercial feed spacers, remains limited to experimental methods. Schock and Miquel [24] used various commercial spacers to measure the mass transfer and pressure drop. They showed that spacer-filled channels have higher mass transfer

compared to empty channels over the same range of Reynolds numbers, albeit at the increased pressure drop. Da Costa et al. [25] studied the effect of spacer filament orientation on the flux enhancement in ultrafiltration membranes. They found a maximum flux for a flow attack angle of 40-45°. In another study [26], they used dye injection and microbubbles to visualize the effects of the spacer's configuration on the flow pattern of spacer-filled channels. They showed that in spacers with a smaller flow attack angle, the flow is more widely spread in the XY-plane (Fig. 1). Neal et al. [5] investigated the orientation effects of commercial feed spacers on particle deposition. They used a spacer with a geometry similar to the standard 28 mil feed spacer used in most SWM modules of RO, albeit in combination with a microfiltration membrane. They [5] linked the deposition patterns of particles to the orientation of feed spacer and the non-uniform shape of the filaments in commercial spacers.

While numerical studies enhance our understanding of hydraulic conditions of spacer-filled channels at relatively low costs and risks compared to experimental methods, they may be associated with challenges such as matching the geometry of the modeled feed spacer with commercial ones and an accurate verification and validation of numerical modules. As a result, it is recommended [27,28] to use direct, non-invasive, high-resolution experimental methods such as Particle Image Velocimetry (PIV). Gimmelshtein and Semiat [29] used PIV for investigation of the liquid flow in the spacer-filled channel in the velocity ranges from 0.06 to 1.3 m/s. They showed that the bulk of fluid flows in a straight line from inlet to outlet with only small deviations near the filaments. Willems et al. [28] investigated the fluid velocity profiles of water and water-air mixture in spacer-filled channels. They found that liquid flows mainly parallel to the spacers' filaments and therefore, the direction of flow changed 90° over the height of the channel. The disagreement of their results with results of Gimmelshtein and Semiat [29] was due to the fact that the latter researchers used a spacer which was 20% thinner than the channel height and thus created an empty space in the channel height. Additionally, the PIV results obtained by Gimmelshtein and Semiat indicate that they may have measured the velocity only in the empty part of the channel. Haidari et al. [11] compared the flow pattern of an empty channel with a spacer filled-channel using PIV. They showed that the flow in the empty channel was in a straight line from inlet to outlet and in the spacer-filled channel, which was in agreement with the results of Willems et al. [28]. In addition, they showed that the low-velocity regions were in agreement with the fouling sites detected by other researchers.

The purpose of this study is to determine the effects of orientation of commercial feed spacers on the fluid flow and the pressure drop. Three different spacers were considered, each at two orientations: normal orientation and ladder orientation (Fig. 1). The effect of orientation on the pressure drop of the same spacers was investigated. A short description of the PIV technique is given in the experimental part of this
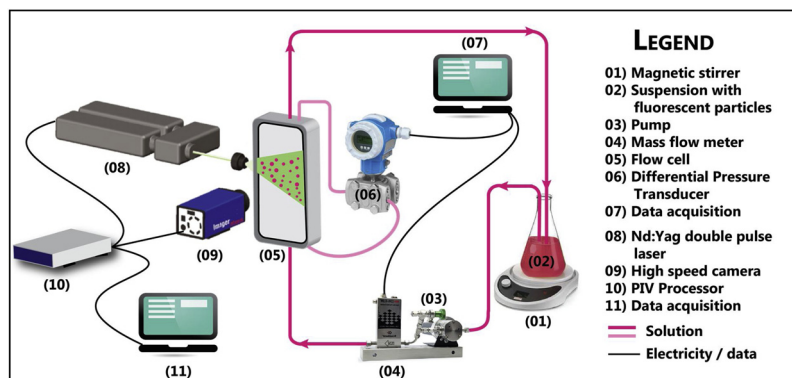

Fig. 2. The experimental setup that was used for measurement of the pressure losses over the flow cell and for visualization of the temporal and spatial velocity variations inside the spacer-filled channel [11,12].

article. The detailed description of the technique is provided by Adrian et al. [30]. The effect of the spacers' orientation on the spatial and temporal velocity variations was studied at three heights of the feed channel. Finally, the flow patterns were compared with fouling sites mentioned by previous studies with the objective of linking the flow pattern with the fouling.

2. Experimental

The experimental setup is shown in Fig. 2. A suspension with fluorescent particles (02) flows through a pump (03) and a mass flow meter (04) to the flow cells (05). The pressure drop over the flow cell is measured by means of a differential pressure transducer (06). The values from the pressure transmitter and from the mass flow meter are used to determine the friction factor. Simultaneously, velocities are measured as the laser (08) emits two light pulses that illuminate a well-defined plane and have a short time interval, synchronized with a high-speed camera (09) that takes two images (11). The captured frames are used to determine the variations of temporal and spatial velocity inside the channel using commercial software (Davis 7.2). A detailed description of the setup can be found in a previous study [11].

The curvature effects of SWM modules on the flow can be neglected because of the small channel height in these modules [18,19] in comparison with the radius. Therefore, it is a common practice to use flat flow cells to study hydraulic conditions of thin spacer-filled channels such as those of SWM modules of RO. The flow cell used in this study (L = 260 mm, W = 85 mm, H = 55 mm) included an embedded flow channel (L = 200 mm and W = 40 mm) for the membrane coupon (Trisep-AMC1) and a spacer. The height of the flow channel is changed according to the spacer thickness by using plastic shims.

The experiments were conducted without the permeate production as the ratio of permeate in RO is small compared to the cross-flow velocity. The non-woven commercial feed spacers (DelStar Technologies, INC.) in this study were made of polypropylene without any further modifications. The geometric specifications of these spacers are given in Table 1. Values of the porosity and hydraulic diameter are respectively calculated by using Eq. (1) [26] and Eq. (2) [26,27].

$$\varepsilon = 1 - \frac{\pi d_f^2}{2 l_m h_{sp} \sin\beta} \tag{1}$$

$$d_H = \frac{4 \times \varepsilon}{\frac{2}{H_{CH}} + (1 - \varepsilon). \, S_{v,SP}} \tag{2}$$

$S_{v,SP}$ represents the specific surface of the feed spacer that can be calculated by dividing the feed spacer surface to volume. The definition of other parameters and symbols is mentioned in the beginning of this article. The same spacer is used at two different orientations: the orientation with the flow attack angle of 45°, which is common in SWM modules of RO and here referred to as the normal orientation, and the orientation with the flow attack angle of 90°, which is not usual in SWM

modules of RO and will be referred to as the ladder orientation.

Experiments are done at constant temperature (< 1% errors from the average temperature [°C]) and different flow rates. Different flow rates were required to determine the dependency of the friction factor (C_{td}) on the Reynolds number (Eq. (3)).

$$C_{td} = \frac{2}{\rho. \, u_{ave}^2}. \, \frac{\Delta p}{L}. \, d_h \propto \frac{A'}{Re_h^n} \tag{3}$$

The dependency of the friction factor on the Reynolds number can be used to determine the flow conditions of the channel. Determining the power "n" of the Reynolds number in the definition of the friction factor, in Eq. (3), gives a better understanding of the flow conditions in the feed channel. A lower value of "n" indicates a higher state of flow disturbance in the channel. Da Costa et al. [26] achieved n-values between $0.16 - 0.34$ for different spacers at velocities that varied between 0.27–2.91 m/s. A' is a constant which is determined by geometry of the spacer and the channel.

The definition used for the Reynolds number here is equivalent to the one used by Schock and Miquel [24] and Fimbres-Weihs and Wiley [27,31] (Eq. (4)).

$$Re_h = \frac{\rho. \, U_{ave}. \, d_h}{\mu} \tag{4}$$

The (hydraulic) Reynolds number is determined as a function of average velocity of the spacer-filled channel (Eq. (5)) and the channel height (H_{CH}).

$$U_{ave} = \frac{Q}{A_{eff}} = \frac{Q}{A. \, \varepsilon} = \frac{Q}{W. \, H_{CH}. \, \varepsilon} = \frac{U_{sup}}{\varepsilon} \tag{5}$$

Other typical definitions for the Reynolds number used in the literature are the channel Reynolds number [32] and the cylinder Reynolds number [8]. The channel and cylinder Reynolds number make use of the average velocity in the empty channel (U_{sup} in Eq. (5)) respectively in combination with channel height and filament diameter. The calculation of average velocity (Eq. (5)) is done with a single average filament thickness value, while the thickness of a manufactured filament in commercial spacers varies over its length.

The state of flow can also be determined by defining the relation between the pressure drop and the power of average velocity in the main direction of flow "m" (Eq. (6)).

$$\Delta p \propto K \times u_{ave}^m \tag{6}$$

It was suggested [33,34] that "m" should be around one for laminar flow and around 1.75 for turbulent. However, in turbulent flow the Reynolds number (Re) is far above the Reynolds number occurring in the SWM modules of RO. Therefore, as it has been suggested [27,35], it is better to talk about the disturbance inside the flow as eddies rather than turbulence.

The velocity in the PIV experiments is determined by capturing two frames that are taken at about 100 mm from the inlet and 15 mm from

Table 1
Geometric characterizations of the commercial spacers used in this study. Each spacer was used in two orientations: normal orientation with a flow attack angle of 45° and ladder orientation with a flow attack angle of 90°.

Description	nomenclature		Ladder Orientation			Normal Orientation		
	Symbol	Unit	A1	B1	C1	A2	B2	C2
Spacer/Channel height	$h_{SP} = H_{CH}$	10^{-3} m	0.71	1.22	1.63	0.71	1.22	1.63
Filament diameter parallel/perpendicular to flow	$d_f = d_{f1} = d_{f2}$	10^{-3} m	0.39	0.8	0.87	0.39	0.8	0.87
Mesh length parallel (perpendicular) to flow	$l_m = l_{m1} = l_{m2}$	10^{-3} m	2.85	4.41	3.86	2.85	4.41	3.86
Hydrodynamic angle	β	o	90	90	90	90	90	90
Flow attack angle	α	o	45	45	45	90	90	90
Aspect ratio	l_m/H_{CH}	–	4.01	3.62	2.38	4.01	3.62	2.38
Relative height	d_f/H_{CH}	–	0.55	0.66	0.54	0.55	0.66	0.54
Porosity	ε	%	88	81	81	88	81	81
Hydraulic diameter	dh	10^{-3} m	0.88	1.26	1.54	0.88	1.26	1.54

each edge of the cell in order to limit the effects of boundaries (entrance, edges and exit) on the flow and to ensure a fully developed flow. The flow along the channel is traced by using fluorescent particles with a mean diameter of 10 μm and a density of 1.19 g/cm^3. The calculated Stokes number of particles was around 5×10^{-3} for the thinnest spacer used (28 mil spacer: 0.71 mm spacer), and thus tracing accuracy errors were below 1% [36]. Fluorescence was used in combination with an optical filter to improve the quality of images. The time interval between two pulses (two frames) was adjusted to the particles displacement in order to reduce loss of particle images within the interrogation window from the first frame to the second frame [11]. An interrogation window or a sub-window is an area smaller than the area of a captured frame, here 7.4×7.4 μm^2, from which information is obtained related to the most probable displacement of the particle pattern in a short time interval.

The PIV measurements were performed at three different heights in the feed channel separately: close to the camera (Z3), in the middle of the channel (Z2), and far from the camera or close to the membrane sheet at the bottom of the feed channel (Z1). The whole depth of the channel was illuminated because the thickness of the laser sheet light (2 mm) was greater than the thickness of the feed channel (0.7 mm). That is a common situation in μPIV [28] and can be solved by fixing the focus of the camera at a specific distance from the lens and moving the object [28,37]. In this study, moving the flow cell was not an option and therefore, the camera was moved on a translation stage (50 μm in each step). The camera was initially placed such that particles in the middle of the channel and close to the membrane were barely in focus (Z3 in Fig. 3). Then the camera was moved to the subsequent positions (Z1, Z2 in Fig. 3) with a translating stage. The camera's depth of field in this setup was about 0.14 mm. At each depth, 50 pairs of images (100 frames) were taken for a specific flow. A instantaneous velocity map is calculated for each pair of frames. These 50 instantaneous velocity maps are used to compare the velocities inside the feed channels over time (temporal velocity). An average is calculated from these 50 instantaneous velocity maps (averaged spatial velocity profile) and is used to study the spatial variations of the velocity inside the feed channel [11].

3. Results and discussions

3.1. Pressure drop and friction losses

Fig. 4 illustrates the dependency of pressure drop (Δp) on average velocity (U$_{ave}$) and dependency of friction factor (C$_{td}$) on hydraulic Reynolds number (Re$_h$). In parallel to PIV measurements, each point in Fig. 4 represents an average of at least 450 measurements. The same feed flow range (1.4–16.0 l/h) was applied to the spacers, and therefore, each feed spacer is operated at a slightly different average velocity range. The range of average velocity in spacers C was slightly lower
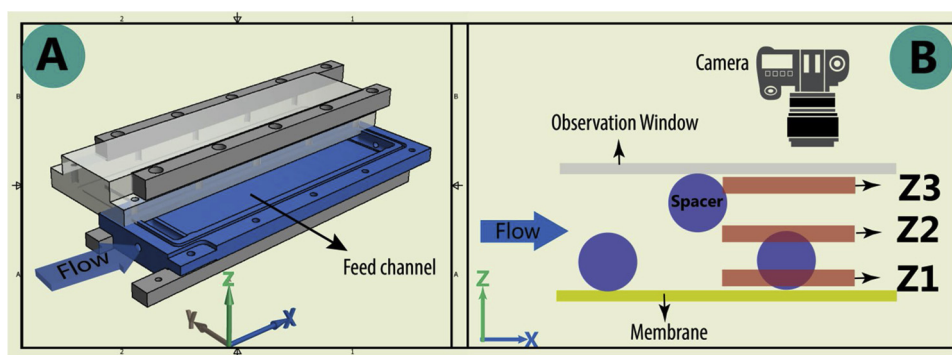

Fig. 4. The variation of pressure drop with the hydraulic Reynolds number (A) and the variation of the friction factor with hydraulic Reynolds number (B). The lines identified with a diamond shape represent the normal orientation, and those identified with a square represent the ladder orientation.

than values commonly used in experimental studies for RO. However, these values are interesting for low salinity water purification in which water permeation could be relatively significant.

As shown in Fig. 4A, the pressure drop over the feed channel is expressed in [bars/m], while the spacers used in the experiments were only 20 cm long. The conversion from 20 cm to one meter is done linearly as it often happens in the practice and it is intentionally expressed in [bars/m] to be able to compare the achieved results with results from practice. For instance, the pressure drop in an RO pressure vessel is calculated by multiplying the number of elements in a pressure vessel by 0.2 bars, which is the pressure drop over one element drives with an average velocity of 0.1 m/s. It is worth mentioning that common spiral wound RO elements are typically one meter long and include spacers with characteristics the same as spacer A$_{Normal}$. The common average velocity in these elements is about 0.1 − 0.3 m/s. Comparing the results from Fig. 4A, with the practical results and results from literature [38] shows that the measured pressure drop represents the actual values in the practice.

Fig. 4A shows that for the experimental conditions in this study, the

Fig. 3. The flow cell used in this study (A) and the cross-section of the flow channel (B) with locations at which PIV measurements are done: Z1 (far from the camera and close to the membrane coupon), Z2 (middle of the channel), and Z3 (close to the camera and observation window).
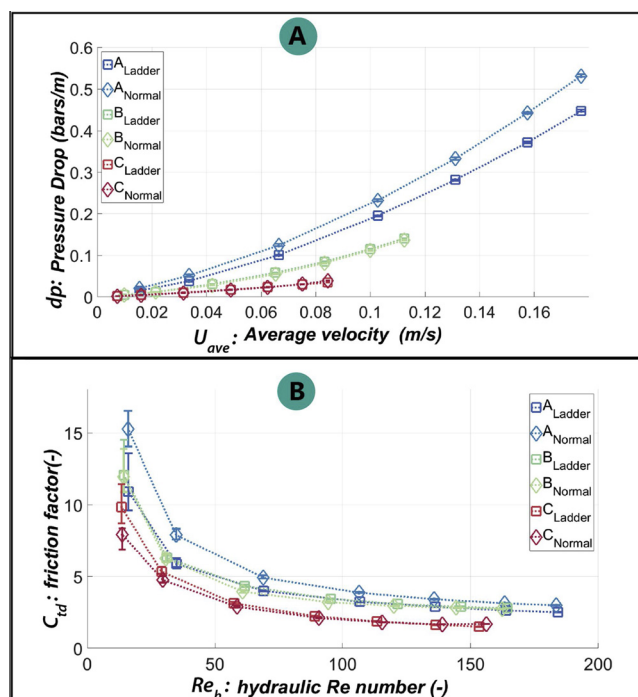
pressure drop differs notably only in two orientations of the spacer A and, as expected, the pressure drop is lower with the ladder orientation. Additionally, Fig. 4A shows that apparently the pressure drop decreases with increasing spacer thickness. However, it is difficult to draw such a conclusion based only on the presented data because the spacers do not change merely in thickness but also in geometric characterizations such as mesh length, hydraulic diameter and porosity. The best fitted values for dependency of the velocity on pressure drop are illustrated in Table 2. Considering only the m-values, the flow is more similar to a Stokes flow in the ladder orientation than in the normal orientation. In addition, the flow with spacer C is more similar to a Stokes flow than other spacers. The n-values, which are obtained from the best fitted data of Fig. 4B, do not match the flow conditions between the two orientations as mentioned earlier. However, the n-values confirm the fact that the flow with spacer C appears more Stokesian than with the two other spacers.

3.2. The actual velocity fields determined by PIV

This section presents the spatial and temporal velocity maps obtained by PIV. In contrast to the average velocity (Eq. (5)), which is normally expressed as a single value, the PIV results are shown in the form of velocity fields or velocity maps. PIV provides information about the velocity development at a particular point in time (temporal velocity). A instantaneous spatial velocity profile is created by measuring the velocity of all the points in the camera's field of view at a particular time step. Averaging all instantaneous spatial velocity profiles results in the averaged spatial velocity profile. Following the line of former studies, the term "average velocity" refers to the theoretically inferred velocity at the feed channel inlet (Eq. (5)) and without considering whether the value is fully developed. The flow becomes fully developed at some distance downstream of the inlet, which is called the entrance length. The entrance length in empty rectangular channels depends on the aspect ratio, defined as the ratio of the channel height to the channel width [39] and is rather small for the setup used in this study (about 2.17 mm). It is, however, challenging to calculate the entrance length in spacer-filled channels. PIV measurements are performed at some distance from the inlet to avoid effects of the entrance length.

Figs. 5–7 illustrate averaged spatial velocity patterns of the ladder and normal orientation in the middle of the channel for an average velocity of 0.1 m/s with spacers A and B and 0.08 m/s with spacer C. Fig. 8 illustrates instantaneous variations of the velocity at a particular point inside a mesh.

3.2.1. Spatial velocity patterns

3.2.1.1. Velocity at the middle of the channel height. Fig. 5 shows averaged spatial velocity profiles for two examined orientations of each spacer at the middle of the channel (Z2 in Fig. 3). The zones with velocity close to zero above the filaments can be used as an indication that the images are taken at the middle part of the channel. However, there is a slightly different scenario in C1 and C2 (respectively the ladder orientation and normal orientation of spacer C). Long arrows, which indicate high velocity regions, appear on top of the filaments mainly close to the nodes of the spacer on the right side of the meshes. This is the result of the non-uniform shape of filaments over their length

in the commercial feed spacer, which is slightly thinner at the places with higher velocity than other parts. At the thinner part, the filament is slightly out of the camera's focus and therefore does not measure the velocity exactly on the filament's surface. This shows that the enhanced geometric characterizations introduced to the numerical studies done by Bucs et al. [22] and Radu et al. [23] is very close to the actual flow behavior as it occurs in a feed channel filled with commercial feed spacers.

Additionally, Fig. 5 shows that the flow in the ladder orientation (type 1) is in a straight line from the inlet to the outlet, while in the normal orientation the bulk flows along the filaments close to it. Local averaged spatial velocities change from very low values up to more than two times the average velocity in some areas. The difference between the low- and high-velocity regions is greater in the ladder orientation than in the normal orientation, comparing different spacers. Velocity values with spacer B1 are highest, reaching almost 0.26 m/s in some places.

In the ladder orientation, a low velocity region is formed downstream of the filaments. This region differs slightly from the particle deposition area, interpreted as a region with low velocity, described by Neal et al. [5], but it was in close agreement with the results of particle deposition achieved by Radu et al. [23] (Fig. 08 in their work). Neal et al. [5] used a spacer with the same geometric characteristics as spacer A, and observed that particles were deposited on the micro-filtration membrane at some distance from the filaments and not directly at the downstream area. This no-deposition area directly downstream of the filaments is explained by the work of Cao et al. [40] who showed that relatively strong eddy currents are present in this area. The difference regarding the presence of the no-deposition zone directly behind the transverse filament between this study and the study done by Neal et al. [5] could be explained by the fact that they used higher flow rates (Re < 400) than in this study (Re < 200).

Notably, the velocity magnitude downstream of filaments with the ladder orientation is not uniform along the entire filament's length, which is probably the consequence of the filament's cross-sectional shape. The highest velocity downstream of a filament is observed at locations where filaments bulge toward the flow. The acceleration effect was more apparent over the swelled part of transverse filaments in thicker spacers than thinner spacers.

In the normal orientation, water passes over the filaments attached to the membrane and under the filaments attached to the observation window and is mixed in the following mesh; this is repeated for every mesh. This complex mixing behavior of the flow together with the particular geometry of each spacer (thickness and porosity) and filaments makes it difficult to give a general prediction of the lowest and highest velocity areas. For instance, in the channel with spacer A, the lowest velocity region is observed in that half of the mesh where the water passes over a filament to enter the mesh and under the adjacent filament to leave the mesh (right half of the meshes in Fig. 5), and the highest velocity is at the other half of the mesh where water passes under a filament to enter the mesh and over a filament to leave the mesh. With spacer B, the highest velocity occurs directly downstream of the filaments at the entering parts of the mesh and the lowest at the confluence of these streams. With spacer C, the lowest velocity occurs in the diagonal part of the mesh. The upstream node of the mesh, where

Table 2
Constants in the total drag dependency on Re-number (A' and n), and the exponent in pressure drop dependency on velocity for the feed spacers used in this study.

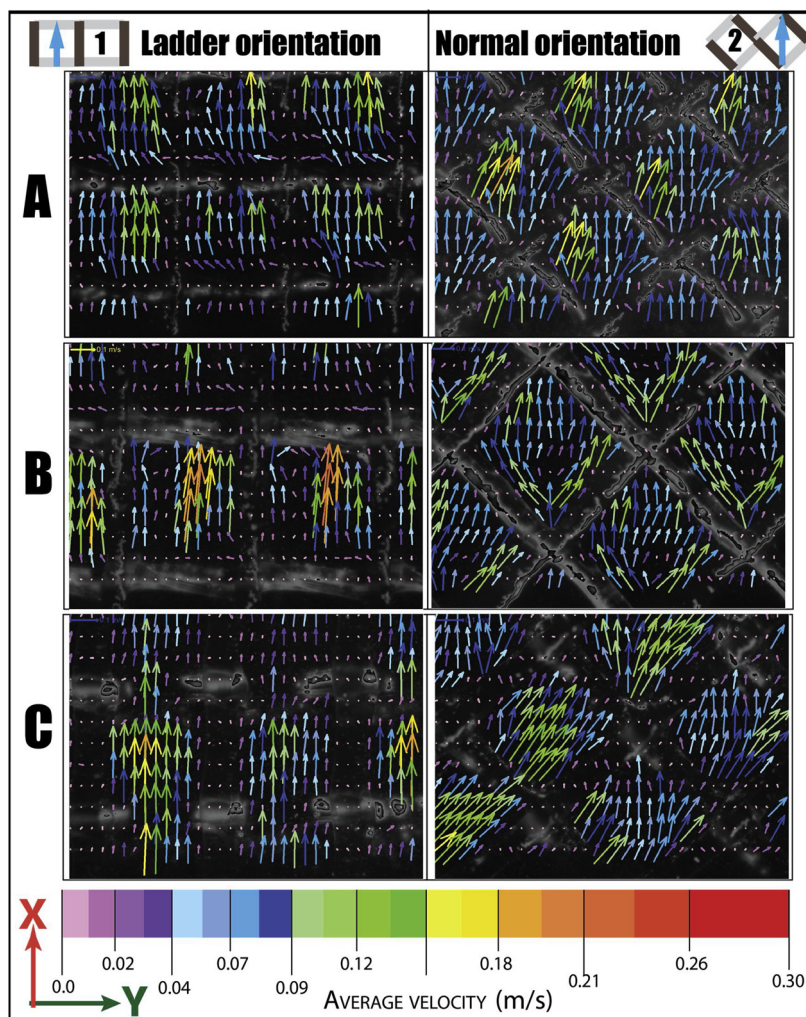| Description	Nomenclature		Ladder Orientation			Normal Orientation		
	Symbol	Unit	A1	B1	C1	A2	B2	C2
Numerator power equation	A'	–	63	66	74	111	70	47
Re power in denominator power equation	n	–	0.64	0.65	0.78	0.72	0.68	0.68
Constant pressure drop dependency on velocity	K	–	6.14	4.4	0.76	6.91	4.94	1.54
Exponent pressure drop dependency on velocity	m	–	1.51	1.58	1.25	1.49	1.65	1.5

Fig. 5. The averaged spatial velocity patterns at the middle of the feed channel (Z2) for the ladder orientation (1) and for the normal orientation (2). The average velocity in spacer C (U_{ave} = 0.085 m/s) is lower than the velocity in spacers A and B (U_{ave} = 0.1 m/s).

both flows exit the mesh, is the only point in all spacers with a similar low-velocity region.

3.2.1.2. Velocity pattern at different channel heights. The velocity patterns as described in the previous section (Fig. 5) are only valid for the situation in which the camera is focused on the middle part of the channel (Z2 in Fig. 3). Fig. 6 shows averaged spatial velocity patterns at the membrane side (Z1 in Fig. 3) on which the transverse filaments are placed. The operational conditions were the same as the operational conditions at the middle of the channel. Velocity magnitudes of the ladder orientation are significantly lower over the membrane side than the middle part of the channel. In addition, the velocity decrease in ladder orientation over the membrane compared to the middle of the channel is greater with thicker spacers. In the normal orientation, the velocity close to the membrane is approximately the same as in the middle of the channel.

The flow direction, on the other hand, differs clearly from the flow direction at the middle of the channel in both orientations. In the normal orientation, the flow is along the direction of attached filaments. In the ladder orientation, the flow direction close to the membrane side is a function of the spacer thickness. For instance, the flow direction with spacer A is approximately the same as in the middle of the channel from the inlet to the outlet with the largest deviation downstream of the filaments. These areas are referred to as the particle deposition area by Neal et al. [5]. The magnitude of the velocity is

respectively 44% and 57% lower for spacer B and C compared to spacer A.

Fig. 7 includes the statistical representation of Figs. 5 and 6, and averaged spatial velocity profile at the front part of the channel (Z1 in Fig. 3), i.e., each box shows the velocity variations over the total field of view at a specific height (Z1, Z2, and Z3 from Fig. 3). The median, average, and outliers are shown respectively with a straight line, empty circle inside the box, and filled circles. Fig. 7 shows that the averaged spatial velocity is higher at the side of the channel without the transverse filaments (Z3) than in the middle of the channel (Z2) in the ladder orientation for the same conditions.

The velocity magnitude at the observation window (Z3) was on average higher, from 3.6% in spacer A to 54% in spacer B, in ladder orientation than in normal orientation. The velocity magnitude at the membrane side (Z1) was lower, from 28% in spacer A to 68% in spacer C, in ladder orientation compared to normal orientation. At the middle of the channel (Z2), the velocity magnitude was lower, from 5% in spacer A to 27% in spacer C, in ladder orientation than in the normal orientation.

The lower velocity at the membrane side of the ladder orientation can be explained by considering the role of transverse filaments. Transverse filaments accelerate the flow at the opposite half of the channel as they are narrowing the flow path. In the normal orientation, both filament layers contribute to flow acceleration, i.e. there are accelerated flows at the top and bottom of the membrane. Because the
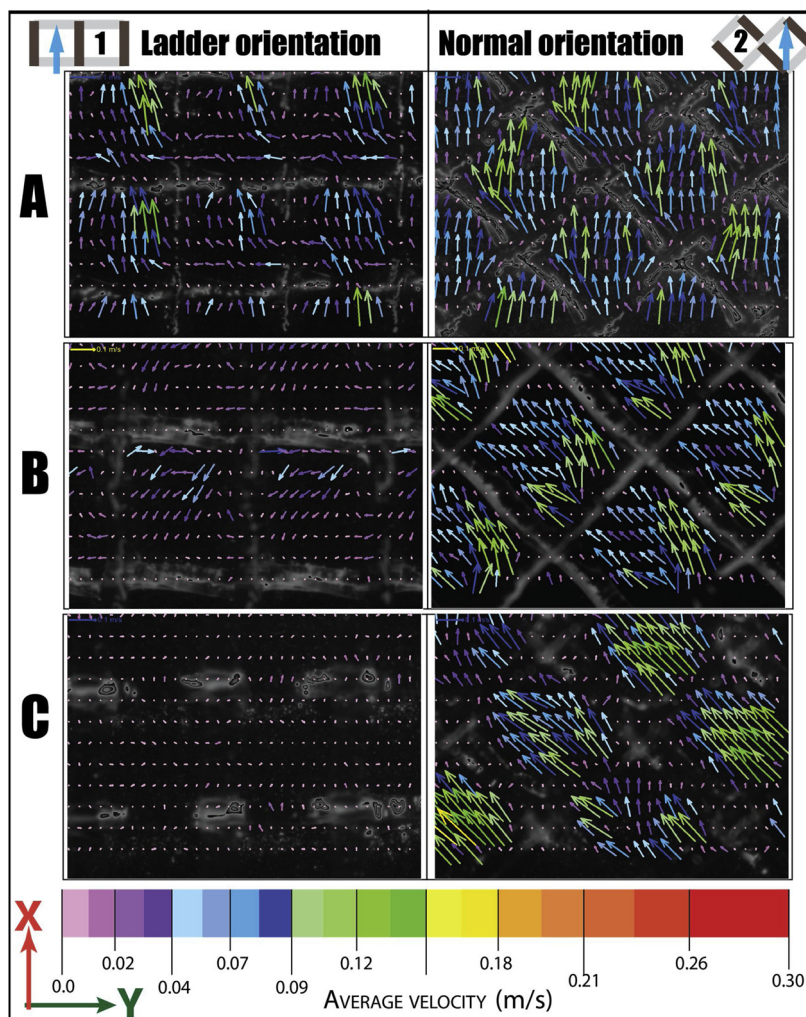
Fig. 6. The averaged velocity pattern close to the membrane side over which the transverse filaments are placed (Z3) for the ladder orientation (1) and for the normal orientation (2). The average velocity in spacer C (U_{ave} = 0.085 m/s) is lower than the inlet velocity in spacer A and B (U_{ave} = 0.1 m/s).
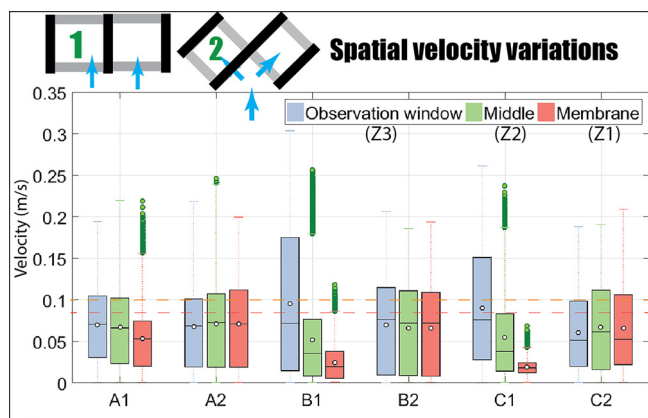

Fig. 7. Spatial variations of averaged spatial velocity profiles at three channel heights for the ladder (1) and normal orientation (2). The average velocity is about 0.1 m/s for spacers A and B and 0.08 m/s for spacer C. The membrane side (Z1) indicates the channel side far from the camera where the transverse filaments are placed in ladder orientation and the observation window (Z3) indicates the channel side close to the camera without transverse filaments in ladder orientation.
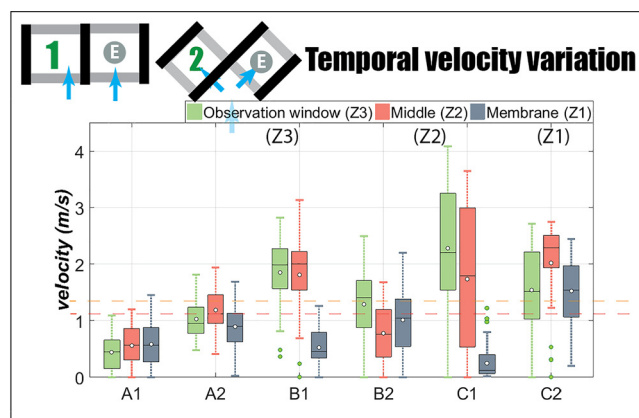
flow attack angle is 45°, top and bottom flows cross each other, and a proper mixing of flow occurs in the feed channel. In the ladder

Fig. 8. Variation of temporal velocity at a point in the middle of a mesh (point E) for an average velocity of 0.1 m/s (spacer A and B) and 0.08 m/s (spacer C).

orientation, where the flow attack angle is 90°, only transverse filaments contribute to flow acceleration, i.e. there is no acceleration due to filaments parallel to the flow on the side that transverse filaments are attached to; therefore, the flow becomes more isolated between two successive filaments, and low-velocity areas are formed.

3.2.2. Temporal velocity variation

Fig. 8 shows variations of the velocity in time for the point "E" in the center of a mesh for three channel heights. The median, average, and outliers are shown respectively with a straight line, empty circle inside the box, and filled circles. In general, the velocity variations for the normal orientation are less than with the ladder orientation, which resembles the averaged spatial profiles as shown in Fig. 7. As expected, the variation in time is greater than in space since the spatial variations are based on time-averaged velocities.

Fig. 8 illustrates that the magnitude and variation of the temporal velocity is clearly lower in ladder orientation compared to the normal orientation, particularly in spacers B and C. Remarkably, with the ladder orientation, the variation of velocity is higher (particularly with spacer B and C) in the middle of the channel (Z2), compared to the observation window (Z3), and at the membrane side (Z1). This is probably the result of a clear separation in the flow magnitude at the top (high velocity) and bottom (low velocity) parts of the flow channel. The high-velocity variations could be the result of vortex shedding in the lee side of filaments or due to the existence of pulsating flow as the consequence of acceleration and deceleration of flow when moving from one mesh to the other one. In either case, high-velocity variation in time is considered beneficial with respect to fouling prevention and concentration polarization destabilization. However, the high-velocity variations observed with the ladder orientation occur in the middle of the channel, while fouling and concentration polarization tend to happen on the membrane sides; the benefit could therefore be minimal in this case. In the normal orientation, the velocity has the same magnitude at the top and bottom parts of the channel because both layers of filaments contribute to the flow acceleration in the channel.

4. Conclusions

In this study, the impacts of two orientations of three spacers with different thicknesses are experimentally assessed with regards to the pressure drop and velocity patterns at three heights in the channel: close to the membrane (Z1 in Fig. 3), close to the observation window (Z3 in Fig. 3), and in the middle of the channel (Z2 in Fig. 3).

The results reveal higher benefits for the ladder orientation compared to the normal orientation only for the case of the thinner spacer. The pressure drop with the ladder orientation was 10% and 17% lower compared to the normal orientation respectively for the thickest (C) and thinnest (A) spacer.

The velocity maps in this study, obtained using Particle Image Velocimetry (PIV), were in agreement with the particle deposition patterns described by Neal et al. [5] and Radu et al. [23].

In general, there was a distinct difference in velocity magnitude for the ladder orientation at three heights in the feed channel, but minor differences with the normal orientation. Moreover, the difference was less evident with the ladder orientation of spacer A than spacers B and C. In addition, the velocity magnitude was enhanced for spacer A in the ladder orientation over the channel height compared to the normal orientation. The same is reported by Neal et al. [5], which is likely because they used a spacer with a similar geometry as spacer A.

In the ladder orientation of spacer B and C, the lowest velocity was observed at the membrane side with attached transverse filaments and the highest at the membrane side without transverse filaments. In addition, the velocity magnitude at the membrane side is decreased with the increase in spacer thickness. Low-velocity regions created at the membrane side with transverse filaments could have a high fouling potential because of low shear stresses in these areas. On the other hand, the high velocity at the membrane side without transverse filaments might not be beneficial, because there is an optimal shear required to prevent fouling, and values above this value will cause increased pressure drop without a significant effect on the fouling remediation. In conclusion, the advantage of ladder orientation is obtained when applied with thinner feed spacers rather than thicker ones.

While our results provide a reasonable estimation of the velocity maps, which are taken at three different heights (Z1, Z2, and Z3) inside the feed channel at different moments (asynchronously), further experimental investigations would be required to quantify the effect of velocity in the Z-direction and associated shear stresses simultaneously with velocity in the X- and Y-direction. It would probably be possible to reconstruct 3D maps of mean velocities from the measured 2D values in this study. However, the reconstructed images would not always be relevant, as they have been captured at different time steps. The findings from this study can be exploited as a validation tool for numerical studies, because of their high resolution ($7.4 \times 7.4 \ \mu m^2$). In addition, they can be used to design an optimum feed spacer for spiral wound membrane modules of RO.

Acknowledgements

References

[1] A.H. Haidari, B. Blankert, H. Timmer, S.G.J. Heijman, W.G.J. van der Meer, PURO: a unique RO-design for brackish groundwater treatment, Desalination (2017).

[2] C. Wong, C.E. Williams, J. Pittock, U. Collier, P. Schelle, World's top 10 rivers at risk, WWF For Living Planet, WWF Global Freshwater Programme, Gland, Switzerland, (2007) March.

[3] A.H. Haidari, S.G.J. Heijman, W.G.J. van der Meer, Optimal design of spacers in reverse osmosis, Sep. Purif. Technol. 192 (2018) 441–456.

[4] L.B. de Chazournes, Fresh Water in International Law, (2013).

[5] P.R. Neal, H. Li, A.G. Fane, D.E. Wiley, The effect of filament orientation on critical flux and particle deposition in spacer-filled channels, J. Memb. Sci. 214 (2003) 165–178.

[6] J. Schwinge, P.R. Neal, D.E. Wiley, D.F. Fletcher, A.G. Fane, Spiral wound modules and spacers: Review and analysis, J. Memb. Sci., Membr. Eng. Special Issue (2004) 129–153.

[7] A.R. Da Costa, A.G. Fane, Net-type spacers: effect of configuration on fluid flow path and ultrafiltration flux, Industrial & Engineering Chemistry Research, American Chemical Society, 1994, pp. 1845–1851.

[8] C.P. Koutsou, S.G. Yiantsios, A.J. Karabelas, Numerical simulation of the flow in a plane-channel containing a periodic array of cylindrical turbulence promoters, J. Memb. Sci. 231 (2004) 81–90.

[9] M. Wilf, Effect of new generation of low pressure, high salt rejection membranes on power consumption of RO systems, American Water Works Association, Membrane Technology Conference (1997).

[10] J. Johnson, M. Busch, Engineering aspects of reverse osmosis module design, Desalin. Water Treat. 15 (2010) 236–248.

[11] A.H. Haidari, S.G.J. Heijman, W.G.J. van der Meer, Visualization of hydraulic conditions inside the feed channel of Reverse Osmosis: a practical comparison of velocity between empty and spacer-filled channel, Water Res. 106 (2016) 232–241.

[12] A.H. Haidari, S.G.J. Heijman, W.G.J. van der Meer, Effect of spacer configuration on hydraulic conditions using PIV, Sep. Purif. Technol. 199 (2018) 9–19.

[13] W.G.J. Van der Meer, Mathematical Modelling of NF and RO Membrane Filtration Plants and Modules, (2003).

[14] J.C. Crittenden, R.R. Trussell, D.W. Hand, K.J. Howe, G. Tchobanoglous, Membrane filtration, MWH's Water Treatment: Principles and Design, third edition, John Wiley & Sons, Inc., 2012, pp. 819–902.

[15] C.C. Zimmerer, V. Kottke, Effects of spacer geometry on pressure drop, mass transfer, mixing behavior, and residence time distribution, Desalination 104 (1996) 129–134.

[16] R. Franks, C. Bartels, A. Anit, Demonstrating improved RO system performance with new Low Differential (LD) technology, Hydranautics, Hydranautics, Oceanside, CA. (2010).

[17] CONWED.Global.Netting.Solutions, Pressure drop, membrane damage and bio-fouling, the primary challenges in reverse osmosis, in: C. Plastics (Ed.), Reverse Osmosis Series, Conwed Plastics, 2019.

[18] V.t. Geraldes, V. Semião, M.N. de Pinho, Flow management in nanofiltration spiral wound modules with ladder-type spacers, J. Memb. Sci. 203 (2002) 87–102.

[19] J.L.C. Santos, V. Geraldes, S. Velizarov, J.G. Crespo, Investigation of flow patterns and mass transfer in membrane module channels filled with flow-aligned spacers using computational fluid dynamics (CFD), J. Memb. Sci. 305 (2007) 103–117.

[20] F. Li, W. Meindersma, A.B. de Haan, T. Reith, Optimization of commercial net spacers in spiral wound membrane modules, J. Memb. Sci. 208 (2002) 289–302.

[21] C.P. Koutsou, S.G. Yiantsios, A.J. Karabelas, A numerical and experimental study of mass transfer in spacer-filled channels: effects of spacer geometrical characteristics

and Schmidt number, J. Memb. Sci. 326 (2009) 234–251.

[22] S.S. Bucs, A.I. Radu, V. Lavric, J.S. Vrouwenvelder, C. Picioreanu, Effect of different commercial feed spacers on biofouling of reverse osmosis membrane systems: a numerical study, Desalination 343 (2014) 26–37.

[23] A.I. Radu, M.S.H. van Steen, J.S. Vrouwenvelder, M.C.M. van Loosdrecht, C. Picioreanu, Spacer geometry and particle deposition in spiral wound membrane feed channels, Water Res. 64 (2014) 160–176.

[24] G. Schock, A. Miquel, Mass transfer and pressure loss in spiral wound modules, Desalination 64 (1987) 339–352.

[25] A.R. Da Costa, A.G. Fane, C.J.D. Fell, A.C.M. Franken, Optimal channel spacer design for ultrafiltration, J. Memb. Sci. 62 (1991) 275–291.

[26] A.R. Da Costa, A.G. Fane, D.E. Wiley, Spacer characterization and pressure drop modelling in spacer-filled channels for ultrafiltration, J. Memb. Sci. 87 (1994) 79–98.

[27] G.A. Fimbres-Weihs, D.E. Wiley, Review of 3D CFD modeling of flow and mass transfer in narrow spacer-filled channels in membrane modules, Chemical Engineering and Processing: Process Intensification, Process Intensification on Intensified Transport by Complex Geometries, (2010), pp. 759–781.

[28] P. Willems, N.G. Deen, A.J.B. Kemperman, R.G.H. Lammertink, M. Wessling, M. van Sint Annaland, J.A.M. Kuipers, W.G.J. van der Meer, Use of Particle Imaging Velocimetry to measure liquid velocity profiles in liquid and liquid/gas flows through spacer filled channels, J. Memb. Sci. 362 (2010) 143–153.

[29] M. Gimmelshtein, R. Semiat, Investigation of flow next to membrane walls, J. Memb. Sci. 264 (2005) 137–150.

[30] R.J. Adrian, Twenty years of particle image velocimetry, Exp Fluids (Experiments in Fluids), Springer-Verlag, 2005, pp. 159–169.

[31] G.A. Fimbres-Weihs, D.E. Wiley, Numerical study of mass transfer in three-dimensional spacer-filled narrow channels with steady flow, J. Memb. Sci. 306 (2007) 228–243.

[32] S.K. In, N.C. Ho, The effect of turbulence promoters on mass transfer − numerical analysis and flow visualization, Int. J. Heat Mass Transf. 25 (1982) 1167–1181.

[33] P. Hickey, C.H. Gooding, Pervaporation processes in the chemical industry, in: B.M. Corporation (Ed.), Proceedings of Sixth International Conference on Pervaporation Processes in the Chemical Industry (1992) 153–169.

[34] R.B. Bird, W.E. Stewart, E.N. Lightfoot, Transport Phenomena, Wiley, 2007.

[35] E. Pellerin, E. Michelitsch, K. Darcovich, S. Lin, C.M. Tam, Turbulent transport in membrane modules by CFD simulation in two dimensions, J. Memb. Sci. 100 (1995) 139–153.

[36] B. McKeon, G. Comte-Bellot, J. Foss, J. Westerweel, F. Scarano, C. Tropea, J. Meyers, J. Lee, A. Cavone, R. Schodl, M. Koochesfahani, Y. Andreopoulos, W. Dahm, J. Mullin, J. Wallace, P. Vukoslavčević, S. Morris, E. Pardyjak, A. Cuerva, Velocity, vorticity, and mach number, in: C. Tropea, A.L. Yarin, J.F. Foss (Eds.), Springer Handbook of Experimental Fluid Mechanics, Springer Berlin Heidelberg, Berlin, Heidelberg, 2007, pp. 215–471.

[37] H. Klank, G. Goranović, J.P. Kutter, H. Gjelstrup, J. Michelsen, C.H. Westergaard, PIV measurements in a microfluidic 3D-sheathing structure with three-dimensional flow behaviour, J. Micromechanics Microengineering 12 (2002) 862.

[38] C.W. Aeijelts Averink, I.T. Dijkstra, J.C. van Dijk, Theorie en modellering van membraanfiltratie, H twee O: tijdschrift voor watervoorziening en afvalwaterbe-handeling 28 (1995) 302–307.

[39] J. Du Plessis, M. Collins, A new definition for laminar flow entrance lengths of straight ducts, N&O Joernaal 25 (1992) 11–16.

[40] Z. Cao, D.E. Wiley, A.G. Fane, CFD simulations of net-type turbulence promoters in a narrow channel, J. Memb. Sci. 185 (2001) 157–176.